This is the peer-reviewed, final accepted version for American Mineralogist, published by the Mineralogical Society of America.
The published version is subject to change. Cite as Authors (Year) Title. American Mineralogist, in press.
DOI: https://doi.org/10.2138/am-2021-7651. http://www.minsocam.org/

"Correction 3"

Oxalate formation by *Aspergillus niger* on manganese ore minerals

Olga Frank-Kamenetskaya[a*], Marina Zelenskaya[b], Alina Izatulina[a], Vladislav Gurzhiy[a], Aleksei Rusakov[a], Dmitry Vlasov[b]

[a]Institute of Earth Sciences, St. Petersburg State University, Universitetskaya Nab 7/9, 199034, St. Petersburg, Russia

[b] Department of Biology, St. Petersburg State University, Universitetskaya Nab 7/9, 199034, St. Petersburg, Russia

*Corresponding author. Tel.: +7 921 3316802; E-mail address: ofrank-kam@mail.ru (O. Frank-Kamenetskaya).

Abstract

Microscopic fungi (micromycetes) play an important role in rock alteration often leading to formation of insoluble biogenic oxalates on rock/mineral surfaces. Oxalate crystallization under the influence of fungus *Aspergillus niger* (one of the most active stone destructors) was studied *in vitro* on two Mn,Ca-bearing minerals of manganese ores: todorokite $(Na_{0.36},Ca_{0.09},K_{0.06},Sr_{0.03},Ba_{0.02})_{0.56}(Mn_{5.53},Mg_{0.47})O_{12}\cdot 3\text{-}4H_2O$ and kutnohorite $(Ca_{0.77},Mn_{0.23})(Mn_{0.74},Fe_{0.14},Mg_{0.11})(CO_3)_2$. The underlying minerals and the products of their alteration were investigated using powder and single crystal X-ray diffraction, optical microscopy, SEM and EDX methods.

It was shown that a more intense leaching of Ca-ions (compared to Mn-ions) from todorokite and kutnohorite leads to an earlier crystallization of calcium oxalates (predominantly whewellite) compared to manganese oxalates (lindbergite, falottaite). Crystallization of manganese oxalates on the surface of kutnohorite occurs in more acidic (compared to todorokite) medium through the formation of mycogenic Mn,Ca-bearing oxides, which are close in composition and structure to

todorokite. The possibility of structural evolution within the manganese oxalate crystalline phases caused by hydration and dehydration processes, which are responsible for changes in proportions of lindbergite and falottaite, derives from similarities between the falottaite and lindbergite structures. The amorphization of falottaite in the temperature range of 70 – 80 °C suggests that formation of linbergite by falottaite dehydration occurs via amorphous precursor.

These results can be used for developing efficient biotechnologies using fungi for industrial enrichment of poor manganese ores and environmental bioremediation.

Keywords: fungal biomineralization, *Aspergillus niger*, manganese oxidation, todorokite, kutnohorite, falottaite, lindbergite, whewellite, weddellite

INTRODUCTION

Microscopic fungi (micromycetes) play an important role in rock alteration often leading to formation of insoluble biogenic oxalates on their surfaces (Sterflinger 2000; Burford et al. 2003; Gadd 2007, 2010; Gadd et al. 2014; Gorbushina 2007; Vlasov et al. 2020). Investigation of these processes contributes to the understanding of biomineralization mechanisms under the influence of lithobiotic microbial community and biogeochemical cycles. These knowledge will create a basis for the potential biotechnological applications using fungi (Gadd 2010; Mulligan et al. 2004; Das et al. 2011, 2015, 2016; Acharya et al. 2004).

Simulation experiments with microorganisms (in particular microscopic fungi) are of great importance since they help obtain the patterns of rock alteration by microbial action and identification of the factors controlling these processes (Sayer et al. 1997; Burford et al. 2006; Wei et al. 2012; Ferrier et al. 2019; Vlasov et al 2020).

Manganese is a technologically important metal that has a few direct primary sources and is often mined in conjunction with other metals (Cu, Ni, and other), as well as from the low-grade manganese ores (Das et al. 2011, 2015; Acharya et al. 2004; Ghosh et al., 2016). Genuine interest in biotechnologies using diverse microbes, which leach manganese and other metals from the ores

including low-grade ores, lies in biomining which is a superior green alternative to the current pyro metallurgical techniques (Mehta et al. 2010, Pattnaik et al. 2019, Acharya et al., 2004, Huerta-Rosas et al, 2020, Ghosh et al., 2016, Mulligan et al., 2004). Microscopic fungi (micromycetes), which are active producers of various organic acids, are often used in bioleaching. For example, the leaching of metals from Indian ocean nodules was produced with *Aspergillus niger* (Mehta et al. 2010), the leaching of manganese from manganese ore with *Penicillium citrinum* (Acharya et al., 2001) and *Aspergillus sp.* (Mohanty et al. 2017), the leaching of heavy metals from mine tailings with *Aspergillus fumigatus* (Seh-Bardan et al. 2012). The biotechnologies for bioremediation of the environment from Mn and other toxic metals are also developed (Mota et al. 2020, Tsekova et al. 2010, Ren et. al. 2009, Barbosa et al., 2016, Das et al., 2015).

The interest of the mineralogical community in studying the bioalteration of Mn-bearing minerals is caused by the significant role of manganese in terrestrial and marine biological systems as it is used by photosynthetic microorganisms for oxygen evolution (Tebo et al. 2005; Ehrlich and Newman 2009). In nature Mn ions occur in 2+, 3+ and 4+ oxidation states. Many microorganisms including micromycetes can oxidize Mn^{2+} from soluble phases followed by the precipitation of $Mn^{3+,4+}$ oxides (Santelli et al. 2011; Wei et al. 2012; Tang et al. 2013; Namgung et al. 2018). Microbial oxidation rate exceeds the abiotic oxidation rate by 5-6 orders of magnitude (Tebo 1991; Morgan 2005). Micromycetes producing oxalic acid can reduce back the $Mn^{3+,4+}$ oxides with the formation of manganese oxalates (Wei et al. 2012; Milova-Ziakova et al. 2016; Ferrier et al. 2019). Manganese oxalate dihydrate, which was approved as a new mineral lindbergite $Mn[C_2O_4]\cdot 2H_2O$ (Atencio et al. 2004), was first found in the thallus of the *Pertusaria corallina* lichen on manganese ore (Wilson and Jones 1984). Manganese oxalate trihydrate (falottaite, $Mn[C_2O_4]\cdot 3H_2O$), is a new mineral found in the Falotta mine manganese deposit in the Swiss Alps by Graeser and Gabriel (2013, 2016) but not yet found in biofilms.

In model experiments fungal manganese oxalates with various H_2O contents were obtained before on rhodochrosite (Sayer et al. 1997), manganese oxides (Wie et al. 2012), manganese

nodules (Ferrier et al. 2019) under the influence of *Aspergillus niger* and *Serpula himantioides*. However, patterns of fungal crystallization of manganese oxalates via complex solubilization and redox processes remain unclear.

The present work investigates fungal alteration of Mn,Ca-bearing minerals of manganese ores: complex oxide todorokite and carbonate kutnohorite, *in vitro*. Todorokite $(Na,Ca,K,Ba,Sr)_{1-x}(Mn^{4+},Mn^{3+},Mg)_6O_{12}\cdot 3\text{-}4H_2O$ is one of the main minerals of Fe-Mn nodules, which accumulate on modern oceans bed and are the largest source of manganese ore (Post 1999; Madondo et al. 2020; Bloise et al. 2020). Carbonate kutnohorite $Ca(Mn,Mg,Fe)(CO_3)_2$ is found in more poor sedimentary manganese carbonate ores (Zak and Povondra 1981; Johnson et al. 2015).

The interest of the present work was focused on the following fungal alterations of todorokite and kutnohorite: (1) the sequence of formation and transformation of calcium and manganese oxalates, morphology of formed crystals and their intergrowths; (2) the evolution of pH of the medium during oxalate crystallization; (3) the mechanisms of influence of composition and properties of underlying mineral substrate on oxalate crystallization; and (4) structural evolution of the manganese oxalates, caused by hydration and dehydration processes.

MATERIALS AND METHODS

Experimental conditions

The fungus *A.niger* (strain Ch 4/07), which we previously used in our works (Sturm et al. 2015; Rusakov et al. 2016; Frank-Kamenetskaya et al. 2019; Zelenskaya et al. 2020), was chosen for the experiment for its strong stone destruction activity (Barinova et al. 2010; Sazanova et al. 2014). The fungus had been isolated from the damaged surface Proconesos marble (Mesozoic age; quarried near Constantinople (Warren 1999)) of a monument column of the “Basilica in Basilica” (Tauric Chersonesos, Crimea). The characterization of the strain was performed in the Research Center "Genomic technologies and cellular biology" of the All-Russian Research Institute of

Agricultural Microbiology. The species identification of the strain was based on the sequence of the ITS region of rDNA (GenBank accession no - KF768341).

The two Mn,Ca- minerals were used as underlying substrates: todorokite (from M.Yu. Nikolaenko collection) which was originally found in an outcrop near Niki-Niki town (West Timor, Indonesia) and kutnohorite (from A.G. Bulakh collection) which was taken from Madan (Pb-Zn(-Ag) ore field (Bulgaria).

The experiment was carried out in liquid Czapek-Dox medium ($NaNO_3$ – 3.0; KH_2PO_4 – 1.0; $MgSO_4 \cdot 7H_2O$ – 0.5; KCl – 0.5; $FeSO_4 \cdot 7\ H_2O$ – 0.015; glucose – 30.0 g/l.) at room temperature with constant pH control of cultural liquid (initial pH value 5.5). Mineral blocks (1x1x0.5 cm) were put on the bottom of plastic Petri dishes and 15 ml of Czapek-Dox liquid medium was added so that the surface of the underlying substrate was completely covered with the nutrient medium. Inoculation was carried out with *A.niger* conidia and mycelium fragments from a 10-day-old fungal culture obtained on Czapek-Dox agar medium. The inoculum was placed on the surface of a liquid culture medium without submerging for better development of the surface culture of the fungus. The duration of the experiments ranged from two days to 20 days. Falottaite (manganese oxalate trihydrate) crystals, suitable for X-ray single crystal diffraction analysis, were obtained after 45 days in a separate experiment. Surfaces of Mn,Ca – minerals after the fungal treatment, precipitates and fungal biofilms formed during the experiment were investigated directly on 2, 4, 5, 6, 8, 14 and 20 days. For comparison, control experiments were carried out in parallel without the participation of fungi. All experiments were performed in triplicate.

METHODS

Mn,Ca-bearing minerals and the products of its alteration were investigated by powder and single crystal X-ray diffraction, optical and scanning electron microscopy as well as energy-dispersive X-ray spectroscopy for elemental analysis.

Optical microscopy. To observe the germination of conidia of the fungus, the mycelium development, the sporification and formation of various crystals Leica optical mono and stereo microscopes with digital photo attachments were used.

Powder X-ray diffraction (PXRD). The determination of phase composition of the products of biomineralization was carried out by means of Bruker «D2 Phaser» powder X-ray diffractometer operated with CuK_α radiation. X-ray diffraction patterns were collected at room temperature in the 2θ range of 5-60° with a step of 0.02° and a counting time of half second per step. A sample holder from a single crystal silica slice was used to eliminate the background noise. Phase identification was carried out using the ICDD PDF-2 database (release 2016).

Thermal behavior of fungal falottaite was examined *in situ* using a Rigaku Ultima IV powder X-ray diffractometer (PXRD, CoKα radiation; 40 kV / 30 mA; Bragg-Brentano geometry; PSD D-Tex Ultra detector). A Rigaku SHT-1500 chamber was employed for experiments in air in the range of +25 – +320 °C; a Pt strip (20×12×2 mm^3) was used as a heating element and sample holder. The temperature steps varied from 5 to 20 °C depending on the temperature range. The heating rate was 2 °C/min. The collection time at each temperature step was about 30 min. The irreversibility of the observed phase transformations was verified by collecting PXRD data on cooling.

Single crystal X-ray diffraction (SCXRD). Single crystal of biogenic falottaite was selected under an optical microscope and mounted on a glass fiber. Data were collected using a Bruker SMART diffractometer equipped with an APEX II CCD area detector operated with monochromated MoK_α radiation (λ[MoK_α] = 0.71073 Å) at 50 kV and 40 mA. Diffraction data were collected at room temperature with frame widths of 0.5° in ω and φ, and exposition of 80s per each frame. Data were integrated and corrected for background, Lorentz, and polarization effects by means of the Bruker programs *APEX2* and *XPREP*. A semi-empirical multi-scan absorption correction was applied using the *SADABS* program (Sheldrick 2013). The unit-cell parameters were refined by least-squares

analysis (Table 1). The structure was solved using dual-space algorithm and refined by means of *SHELX* programs (Sheldrick 2015a; 2015b) incorporated in the *OLEX2* program package (Dolomanov et al. 2009). The final model included coordinates and anisotropic displacement parameters for all non-H atoms. Positions of H atoms of H_2O molecules were localized from difference Fourier maps and refined with individual isotropic thermal displacement parameters. Supplementary crystallographic data have been deposited in the Inorganic Crystal Structure Database (CSD 1791378) and can be obtained from Fachinformationszentrum Karlsruhe via https://www.ccdc.cam.ac.uk/structures/.

Scanning electron microscopy (SEM) and Energy-dispersive X-ray (EDX) spectroscopy. Scanning electron microscopy (SEM) with elemental composition analysis was used for identification of oxalate phases by morphological characteristics, examination of morphology of the formed crystals and their intergrowths and also for determination of the elemental composition of underlying substrate and crystallized products. The study was carried out by means of a TM 3000 (HITACHI, Japan, 2010) with OXFORD EDX module. For EDX measurements the microscope was additionally equipped with the Oxford Inca system which operated in a low vacuum (60 Pa) mode and at an acceleration voltage of 15 kV. To avoid the charging effect on SEM images the samples were coated by a thin carbon layer (High Vacuum Carbon Sprayer Q150TE). The EDX spectra were analyzed by means of the EDAX Genesis software package (semiquantitative analysis was performed by standard-less method that is generally reliable for elements with $Z > 10$). Quantitative elemental composition of underlying mineral substrates was analysed on the epoxy-mounted, polished, and carbon-coated samples by means of Hitachi S-3400N scanning electron microscope equipped with AzTec Energy 350 energy dispersive (EDX) spectrometer, using the following analytical standards: pure manganese (Mn), anorthite (Ca), forsterite and MgO (Mg), pure iron (Fe), albite (Na), orthoclase (K), celestine (Sr) and barite (Ba). EDX spectra were obtained under 25 kV accelerating voltage and 10 nA beam current.

Todorokite mineral formula was calculated assuming Mn+Mg content equal to 6. Kutnohorite mineral formula was calculated assuming summarized amount of cations (Ca, Mg, Mn and Fe) equal to 2.

RESULTS

Mineral and elemental composition of underlying substrates

According to PXRD results, it was confirmed that the used mineral substrates are todorokite (ICDD (PDF-2) №01-087-0389) and kutnohorite (ICDD (PDF-2) №01-084-1291). Since manganese oxides with tunnel crystal structure (minerals coronadite, romanechite, todorokite) are usually difficult to analyze due to poor crystallinity (Bish and Post 1989) and may undergo changes during annealing, the manganese oxide sample was studied via PXRD at room temperature (25° C) and after annealing at 100° C and 500° C. No changes in powder XRD patterns were observed, confirming that this substrate corresponds to todorokite (Naganna 1963; Bish and Post 1989; Ghodbane et al. 2010).

According to EDX data (Table 2) formulas for the underlying minerals were: todorokite — $(Na_{0.36},Ca_{0.09},K_{0.06},Sr_{0.03},Ba_{0.02})_{0.56}(Mn_{5.53},Mg_{0.47})O_{12}\cdot 3\text{-}4H_2O$;

kutnohorite — $(Ca_{0.77},Mn_{0.23})(Mn_{0.74},Fe_{0.14},Mg_{0.11})(CO_3)_2$.

Alteration of Ca,Mn-bearing minerals under fungal treatment

Crystallization on a todorokite surface

Alteration of todorokite under fungal treatment was registered already on the 2nd day of the experiment by decrease in pH of the medium (from 5.5 to 4). The beginning of dissolution of the underlying substrate and oxalate crystallization were detected. Numerous groups of lamellar pseudohexagonal crystals of monoclinic whewellite (monohydrate calcium oxalate, $Ca[C_2O_4]H_2O$) were visible on the surface of todorokite, the splitting of which led to the formation of dense stacked intergrowths. Tetragonal weddellite (dihydrate calcium oxalate, $Ca[C_2O_4]\cdot(2.5–x)H_2O$),

was present in the form of single dipyramidal crystals (15-20 μm), some of which also showed signs of intensive splitting (Fig.1a,b; 2a, Table 3).

On the 4th day of the experiment, the pH of the medium did not change. Along with numerous crystals of calcium oxalates (predominantly whewellite) and their intergrowths, monoclinic lindbergite appears, which represented by separate large spherulite-like (shard-like, Ferrier et al. 2019) intergrowths of platy crystals (the size of intergrowths reaches 80-100 μm) (Fig. 1c,d, Table 3). The size of weddellite crystals (~100 μm) and the intensity of their splitting increased. In addition, small (~ 15–20 μm) crystals of weddellite of the next generation were visible.

On the 6th day of the experiment, the pH of the medium decreased to 3.5, the amount of lindbergite increased and a significant amount of orthorhombic falottaite was observed (Figs. 1e, 1f and 2b). The sizes of intergrowths of platy crystals of lindbergite reached 200-250 μm. Falottaite was represented by flat needle crystals, often forming star shaped intergrowths (Fig. 1f inset). The length of the crystals of falottaite varied from 200 μm to 1 mm. The morphology and ratio of calcium oxalates (weddellite and whewellite) preserved the same.

On the 8th day of the experiment a slight increase of pH of the medium (up to 4.5) was recorded. Numerous needle-like crystals of falottaite were visible (Fig.1g,h; 2c). Lindbergite disappeared. The morphology and ratio of calcium oxalates preserved the same.

On the 14th day of experiment pH increased to 6.0, and lindbergite appeared again (the size of the intergrowths of platy crystals ranged from 80 to 180 μm) (Figs. 1i, 1j and 2d). The amounts of lindbergite and falottaite were comparable. Whewellite was represented not only by stacks of platy crystals, but also by their spherulite-like intergrowth aggregates (Fig. 1j inset).

Calcium oxalates, which were present on todorokite at all stages of the experiment, contained an admixture of strontium, while manganese oxalates contained an admixture of magnesium. According to EDX, the content of strontium in calcium oxalates increased during the experiment and the content in weddellite was always greater than in whewellite. The Sr/Ca atomic

ratio in whewellite reached 12%, in Sr-weddellite - 58%, which corresponds to the solid solution $(Ca,Sr)[C_2O_4]\cdot(2.5–x)H_2O$ (sp.gr. I4/m) (Rusakov et al 2019). The Mg amounts in manganese oxalates of various hydration states were comparable. The Mg/Mn atomic ratio in lindbergite reached 15%, in falottaite- 12%.

Crystallization on kutnohorite surface

On the 2nd day of the experiment pH of the medium decreased to 3.5. On the SEM images, along with intensive dissolution of the substrate, a carpet of small pseudo-hexagonal plate crystals of whewellite (from 7 to 15 μm) and whewellite intergrowths (in the form of rosettes and crosses) were visible (Figs. 3 a,b,Table 3).

On the 4th day of the experiment pH of the medium decreased to 3.0. In addition to a continuous carpet of whewellite crystals, biogenic manganese oxide, whose X-ray diffraction pattern was close to that of the todorokite (Fig. 4a), was recorded.

On the 6th day of the experiment pH of the medium decreased to 2.5. Lindbergite and falottaite were present in a significant and comparable amount (Figs. 3c,d; 4b), and the crystals sometimes grew into each other (Fig. 3c, bottom inset). Among the numerous crystals of whewellite (carpet on the surface of the underlying substrate), individual dipyramidal weddellite crystals (15–25 μm) appeared (Fig. 3d). The morphology of whewellite crystals did not change. Lindbergite was represented by both large spherulite-like intergrowths from numerous plate crystals (from 100 to 200 μm) and smaller intergrowths from 2-3 plate crystals (~ 20-30 μm) (Fig. 3c - upper inset). The morphology of the falottaite crystals was similar to that described above on the surface of todorokite.

On the 8th day of the experiment pH reached a minimum value of 2. The surface of the kutnohorite was still covered with a continuous carpet of platy whewellite crystals. Falottaite disappeared, large intergrowths of platy lindbergite crystals were visible (up to 250-300 μm), as

well as individual small platy lindbergite crystals of the following generations (~ 10-60 μm) (Figs. 3e, 4c).

Further, on the 14th and 20th day of the experiment pH slightly increased to 2.5. As shown in the SEM images, almost no changes occurred (Fig. 3 f; 4d).

Manganese oxalates formed on kutnohorite at all stages of the experiment contain impurities of magnesium and iron. The Mg/Mn and Fe/Mn atomic ratios in lindbergite reached 45 and 21%, respectively; in falottaite – 13 and 14%, respectively.

Thermal behavior of biogenic falottaite

High temperature XRD studies of the manganese oxalate trihydrate (falottaite) demonstrated that amorphization process occured in the temperature range of 70 – 80 °C followed by disappearance of fallotaite diffraction peaks (Fig. 5). The previously reported transformation of falottaite to lindbergite (Huizing et al. 1977; Baran 2014), which occurs at room temperature in air during several days, was not observed. At temperatures above 130 °C, broad paeks, probably of manganese oxide (Mn_2O_3) appeared (Donkova and Mehandjiev 2004).

Refinement of biogenic falottaite crystal structure

Our SC XRD measurements showed that the structure of biogenic falottaite formed in the presence of fungus *A.niger* (Fig 6a, c) was identical to that of synthetic manganese oxalate trihydrate (Fu et al. 2005); the latter had been crystallized from an aqueous solution of $MnCO_3$ and oxalic acid (Table S1). According to the similarity of the unit cell parameters (Table S1), both synthetic crystals were structural analogs of mineral falottaite which had originally been found in Falotta ore field (Tinzen, Switzerland) (Graeser and Gabriel 2013).

The distinctive feature of the biogenic falottaite crystals studied here is partial Mn^{2+} to Mg^{2+} ionic substitution: Mn site-scattering factor = 23.1 *epfu*, so the Mn:Mg ratio = 0.85:0.15, which is in

good agreement with the aforementioned EDX result. The structural formula of the falottaite obtained by *A.niger* after 45 days of experiment is $[Mn_{0.85}Mg_{0.15}\ [C_2O_4](H_2O)_2]\cdot(H_2O)$.

DISCUSSION

Regularities of fungal oxalate formation

The results of our *in vitro* experiment demonstrated that the alteration of Mn,Ca-bearing minerals (todorokite and kutnohorite**)** under the influence of *A.niger* fungus occured via a complex of solubilization and crystallization processes, leading to the formation of Ca- and Mn-bearing oxalates with various H_2O contents (analogs of whewellite, weddellite, lindbergite and falottaite). Proportions of lindbergite and falottaite changed as a result of the hydration and dehydration processes.

Other elements that had got into the crystallization medium from the underlying mineral substrate during solubilization were incorporated in Ca- and Mn-oxalates as isomorphic impurities: Sr into weddellite and whewellite (Sr/Ca ≤ 58 and 12%, respectively); Mg and Fe into lindbergite and falottaite (Mg/Mn ≤ 45 and 13%, Fe/Mn ≤ 21 and 14%, respectively).

Calcium oxalates (predominantly whewellite) formed on a surface of todorokite and kutnohorite earlier than manganese oxalates (already on the 2nd day of the experiment) (Table 3, Fig. 1ab, 3ab), which indicates that Ca^{2+} ions were leaching from underlying substrates under the action of aggressive metabolites *A.niger* more intensively than that for manganese ions. Kutnohorite surface was covered with calcium oxalate crystals almost completely, while todorokite surface - only for 30-40%, which may be attributed to the much lower content of Ca^{2+} ions in todorokite than in kutnohorite (Table 2). Significant predominance of whewellite over weddellite on the surface of both substrates at all stages of the experiment (weddellite on the surface of kutnohorite in the early stages could not be detected at all) indicates the prevalence of oxalate ions over calcium ions in the crystallization medium (Kuzmina et al. 2019).

Formation of calcium oxalates on todorokite and kutnohorite started in an acidic medium at almost the same pH values (4 and 3.5, respectively; Table 3; Fig. 7), slightly decreased in

comparison with the initial pH value of 5.5. The pH values on the surface of both underlying substrates during the experiment, first, decreased and then, after having reached a certain limiting value, increased, which may be associated with a decrease of oxalate ions content in solution due to intense crystallization and also with aging of fungus culture (Sturm et al. 2015). The minimum pH value (3.5) at the surface of todorokite, was reached on the 6th day of the experiment, and on the 14th day it increased to 6.0. The minimum pH value (2.0) at the surface of kutnohorite was reached on the 8th day of the experiment, which subsequently increased but very slightly (on the 14th day it was equal to 2.5). Such differences indicate a lower solubility of kutnohorite (as compared with todorokite) in the products of microbial metabolism, which slows down the processes of Mn leaching and Mn-oxalate crystallization that occurs in a more acidic (compared to todorokite) medium.

Formation of manganese oxalates on the surface of Mn,Ca-bearing minerals under the influence of *A.niger* fungus occured *via* complex redox processes (Mn^{2+} to $Mn^{3+,4+}$ and *vice versa*) which depend on the oxidation state of manganese ions in the underlying mineral substrate and on the pH of crystallization medium (Table 3; Fig. 7).

As a result of todorokite solubilization under the influence of fungus, $Mn^{3+,4+}$ ions were directly released into the medium. Then ions were reduced to Mn^{2+} along with the gradual pH increase from 3.5 to 6 which lead to manganese oxalates precipitation starting from dihydrous linbergite formation (Fig. 1c,d, 2c). Later, trihydrous falottaite appeared on the surface of todorokite. The ratio between lindbergite and falottaite varied depending on hydration and dehydration processes (Fig.1c,d,e,f,g,h). Orthorhombic magnesium oxalate dihydrate γ-$Mn(C_2O_4)\cdot 2H_2O$, which is stable according to Huizing et al. (1977) under pH > 4, in the products of the interaction between *A.niger* and todorokite was not found, which can be explained by the stabilizing action of the chemical components of the crystallization medium on the todorokite surface.

During kutnohorite solubilization Mn^{2+} ions were released into the medium and afterwards oxidize to Mn3+,4+ at pH=2.5-3.0, which resulted in the mycogenic Mn,Ca-oxide formation on the 4th day of the experiment. The PXRD pattern of this oxide was close to that of todorokite (Figs. 4a,b). This result is in a good agreement with previous studies, according to which fungal Mn(II) oxidation leads to the formation of Mn(IV)-oxides (Santelli et al. 2011; Wei et al. 2012; Milova-Ziakova et al. 2016; Tang et al. 2013; Namgung et al. 2018). Kutnohorite solubilization in current experiments resulted in the appearance of Mn^{2+} along with Ca^{2+}, Fe^{2+} and Mg^{2+} cations in the crystallization medium, which made it possible to form fungal Mn,Ca-bearing oxide that was close in composition and structure to todorokite. Then Mn,Ca-bearing biogenic oxide solubilized under the influence of micromycetes and $Mn^{3+,4+}$ ions oxidized back to Mn^{2+}. Mn oxalate crystallization started only after that, on the 6^{th} day of the experiment (later than on the todorokite), at the average pH = 2.5. First, lindbergite and falottaite were present on the surface of kutnohorite (Fig3c,d,4b), and then (on the 8^{th} day of the experiment, at the pH = 2), falottaite transformed to lindbergite due to dehydration (Fig.3e,4c). Thus, the acidic medium did not contribute to the stabilization of the manganese oxalate trihydrate, falottaite.

Wei et al. (2012) proposed that lindbergite solely forms due to falottaite dehydration. Our results on kutnohorite supported the possibility of falottaite to lindbergite transformation. High temperature XRD studies of the falottaite demonstrated that amorphization process occured in the temperature range of 70 – 80 °C (Fig. 5). This suggested that falottaite — lindbergite transformation occurs via amorphous precursor phase, that is typical for many carbonate and phosphate minerals of biogenic origin (Yao et al. 2017; Addadi and Weiner 2014; Kim et al. 2019). Additionally, our experiments on todorokite demonstrated the possibility of falottaite formation *via* lindbergite hydration. Lindbergite (and possibly falottaite) had also precipitated directly from solutions on both Mn,Ca-bearing underlying mineral substrates.

As in other model experiments performed with the participation of fungus *A.niger* (Sayer et al. 1997; Wie et al. 2012; Sturm et al. 2015; Rusakov et al. 2016; Ferries et al. 2019; Frank-

Kamenetskaya et al. 2019; Zelenskaya et al. 2020), most oxalate crystals synthesized by us were characterized by multiple splitting and the formation of spherulite-like (shard-like according to Ferrier et al. 2019) and other aggregates (Figs. 1,3), which were absent for manganese and calcium oxalates found in biofilms on the surface of rocks (Wilson and Jones 1984; Frank-Kamenetskaya et al. 2019). Besides, the size of synthesized crystals was significantly larger than that of natural samples. For instance, intergrowths of plate crystals of lindbergite (~300 μm) (Fig. 3f) were significantly larger than that of natural, poorly crystalline phases (5-20 μm) (Wilson and Jones 1984). In our experiments only crystals of lindbergite and weddellite of subsequent generations (small lamellar and dipyramidal, respectively) (Figs. 1cd, 3f) had the morphology close to oxalates from natural biofilms. These differences in morphology between natural crystals and those obtained *in vitro* under the fungus action indicate that the ionic supersaturation of the solutions and the crystal growth rates under natural conditions were not as high as in experiments.

Structural evolution within the manganese oxalates derived by hydration and dehydration processes

The peculiarities of the crystal structures of falottaite and lindbergite minerals make the formation of lindbergite from falottaite possible and *vice versa*. Both structures are based on Mn-centered octahedra linked together *via* oxalate groups into infinite chains, which are in turn arranged to form a pseudo layered architecture (Fig. 6).

Cis-arrangement of $H_2O(2)$ molecules in falottaite results in distorted octahedral coordination of Mn sites (Table S2) which are linked *via* oxalate groups into infinite zigzag chains running along the *a* axis (Fig. 6a). The chains are arranged into pseudo layers parallel to the (010) plane linked together *via* H-bonding between the $H_2O(2)$ molecules and O(3) atoms of oxalate groups from the neighbour chains (Fig.6a, Table S3). Another nonequivalent $H_2O(4)$ molecule situates between the Mn-oxalate pseudo layers providing their linkage into a three-dimensional structure (Fig 6c).

Distorted Mn-centered octahedra in the structure of lindbergite are linked *via* oxalate groups into infinite chains along the *c* axis and are also held together by O—H···O hydrogen bonds (Table S1, Fig. 6b). Two H_2O molecules that coordinate Mn atoms are *trans*-arranged. Both structures are characterized by the absence of vacancies in the sites of O atoms related to H_2O molecules, which is, for instance, different with respect to calcium oxalate weddellite, where the amount of H_2O molecules may vary (Izatulina et al. 2014; Frank-Kamenetskaya et al. 2016; Mills and Christy 2016). The main difference between the structures of monoclinic lindbergite (Deyrieux et al. 1973; Soleimannejad 2007; Echigo 2008) and orthorhombic falottaite is the presence of the interlayer H_2O molecules in the structure of the latter (Fig. 6d). Structural similarities between manganese oxalates with different H_2O contents confirm the possibility of structural evolution within the manganese oxalate crystalline phases caused by hydration and dehydration processes, as also occurs in calcium oxalates (Izatulina et al. 2018).

IMPLICATIONS

The present work contributes to the studies of biomineralization mechanisms under the influence of lithobiont microbial community, primarily fungi. The results of the *in vitro* experiment made it possible to significantly advance in the study of Ca,Mn-bearing minerals bioalteration via a complex of solubilization, crystallization and transformational processes, and showed a significant effect of the composition and properties of the underlying mineral substrate on these processes. The *in vitro* regularities of oxalate crystallization (variations in phase composition of the obtained crystals, their morphology, the incorporation of isomorphic impurities) on the surface of Ca,Mn-bearing minerals under the action of the *A.niger* fungus can now be used for describing the crystallization processes occurring in nature with the participation of micromycetes on surfaces of various minerals, primarily containing ions of transition metals of variable valence (Cu, Fe etc.).

The *in vitro* results obtained using *A.niger* (collected in nature) can be useful for developing new more economical and environmentally friendly efficient biotechnologies using fungi for

manganese leaching from the ores, including low-grade industrial beneficiation of poor manganese ores, and also environmental Mn bioremediation. In particular, the revealed characteristics of the underlying mineral substrate (primarily oxidation state of manganese ions, density and solubility of rock), which directly affect the intensity of solubilization, allow a controlled approach to selecting conditions for bioleaching of manganese from the processed ores.

ACKNOWLEDGMENTS

This work was supported by Russian Science Foundation (project N 19-17-00141).

The laboratory researches were carried out in the Research Park of Saint Petersburg State University, the SEM investigations — in the "Resource Center Microscopy and Microanalysis (RCMM)" and in the Centre for Geo-Environmental Research and Modelling (Geomodel), the XRD measurements — in the X-ray Diffraction Centre.

REFERENCES CITED

Acharya, C., Kar, R.N., Sukla, L.B. (2003) Studies on reaction mechanism of bioleaching of manganese ore. Minerals Engineering, 16, 1027–1030.

Acharya, C., Kar, R.N., Sukla, L.B., Misra V.N. (2004) Fungal leaching of manganese ore. Trans. Indian Inst. Met., 57(5), 501-508.

Addadi, L., Weiner, S. (2014) Biomineralization: mineral formation by organisms. Physica Scripta, 89, 098003.

Atencio, D., Coutinho, J.M.V., Graeser, S., Matioli, P.A., Menezes Filho, L.A.D. (2004) Lindbergite, a new manganese oxalate dihydrate from Boca Rica mine, Galiléia, Minas Gerais, Brazil, and Parsettens, Oberhalbstein, Switzerland. American Mineralogist, 89, 1087-1091.

Baran, E. (2014) Review: Natural oxalates and their analogous synthetic complexes. Journal of Coordination Chemistry, 67(23–24), 3734–3768.

Barbosa, R., Guerra-Sa, R., Lero, V.A. (2016) Mechanisms of manganese bioremediation by microbes: an overview. J Chem Technol Biotechnol, 91, 2733–2739.

Barinova, K.V., Vlasov, D.Yu., Schiparev, S.M., Zelenskaya, M.S., Rusakov, A.V., Frank-Kamenetskaya, O.V. (2010) Production of organic acids by micromycetes from the rock substrates. Mycology and Phythopathology, 44, 137–142 (in Russian).

Bloise, A., Miriello, D., De Rosa, R., Vespasiano, G., Fuoco, I., De Luca, R., Barrese, E., Apollaro, C. (2018) Mineralogical and Geochemical characterization of asbestiform todorokite, birnessite, and ranciéite, and their host mn-rich deposits from Serra D'Aiello (Southern Italy) Fibers, 6.

Bish, D.L., Post, J.E. (1989) Thermal behavior of complex, tunnel-structure manganese oxides. American Mineralogist, 74, 177-186.

Burford, E.P., Kierans, M., Gadd, G.M. (2003) Geomycology: fungi in mineral substrata. Mycologist, 17, 98-107.

Burford, E.P., Hillier, S., Gadd, G.M. (2006) Biomineralization of fungal hyphae with calcite ($CaCO_3$) and calcium oxalate mono- and dihydrate in carboniferous limestone microcosms. Geomicrobiology Journal, 23, 599–611.

Das A.P., Ghosh S., Mohanty S., Sukla L.B. (2015) Advances in manganese pollution and its Bioremediation. In L.B. Sukla et al. Eds., Environmental Microbial Biotechnology, Soil Biology 45, 313-328.

Das A.P., Sukla L.B., Pradhan N., Nayak S. (2011) Manganese biomining: A review. Bioresource Technology, 102, 7381–7387.

Deyrieux, R., Berro, C., Peneloux, A. (1973) Contribution a l'etude des oxalates de certainsmetaux bivalents. III. Structure cristalline des oxalates dihydrates de manganese, de cobalt, de nickel et de zinc. Polymorphisme des oxalates dihydrates de cobalt et de nickel. Bulletin de la Societe Chimique de France, 1, 25-34 (in French).

Donkova, B., Mehandjiev, D. (2004) Mechanism of decomposition of manganese(II) oxalate dihydrate and manganese(II) oxalate trihydrate. Thermochimica Acta, 421, 141–149.

Dolomanov, O.V., Bourhis, L.J., Gildea, R.J., Howard, J.A.K., Puschmann, H. (2009) OLEX2: A complete structure solution, refinement and analysis program. Journal of Applied Crystallography, 42, 339-341.

Echigo, T., Kimata, M. (2008) Single-crystal X-ray diffraction and spectroscopic studies on humboldtine and lindbergite: weak Jahn–Teller effect of Fe^{2+} ion. Physics and Chemistry of Minerals, 35, 467-475.

Ehrlich, H.L., Newman, D.K. (2009) Geomicrobiology, 5th ed., 606 p. Boca Raton; London: CRC Press.

Ferrier, J., Yang, Y., Cseteny, L., Gadd, G.M. (2019) Colonization, penetration and transformation of manganese oxide nodules by *Aspergillus niger*. Environmental Microbiology, 21,1821-1832.

Frank-Kamenetskaya, O.V., Izatulina, A.R., Kuzmina, M.A. (2016) Ion substitutions, non-stoichiometry, and formation conditions of oxalate and phosphate minerals of the human. In O.V. Frank-Kamenetskaya, E.G. Panova, D.Yu. Vlasov, Eds., Biogenic-Abiogenic interactions in natural and anthropogenic systems, p. 425-442. Springer International Publishing, Switzerland.

Frank-Kamenetskaya, O.V., Ivanyuk, G.Y., Zelenskaya, M.S., Izatulina, A.R., Kalashnikov, A.O., Vlasov, D.Yu., Polyanskaya, E.I. (2019) Calcium oxalates in lichens on surface of apatite-nepheline ore (Kola Peninsula, Russia). Minerals, 9, 656.

Fu, X., Wang, C., Li, M. (2005) Catena-Poly[[[diaquamanganese(II)]-μ-oxalato] monohydrate], Acta Crystallographica Section E Structure Reports, 61, m1348-m1349.

Gadd, G.M. (2007) Geomycology: biogeochemical alterations of rocks, minerals, metals and radionuclides by fungi, bioweathering and bioremediation. Mycological Research, 111, 3-49.

Gadd, G.M. (2010) Metals, minerals and microbes: geomicrobiology and bioremediation. Microbiology, 156, 609–643.

Gadd, G.M., Bahri-Esfahani, J., Li, Q., Rhee, Y.J., Wei, Z., Fomina, M., Liang, X. (2014) Oxalate production by fungi: significance in geomycology, biodeterioration and bioremediation. Fungal Biological Reviews, 28, 36–55.

Ghodbane, O., Pascal, J.L., Fraisse, B., Favier, F. (2010) Structural in situ study of the thermal behavior of manganese dioxide materials: toward selected electrode materials for supercapacitors. ACS Applied Materials and Interfaces, 2, 3493-3505.

Ghosh, S., Mohanty, S., Akcil, A., Sukla, L.B., Das A.P. (2016) A greener approach for resource recycling: Manganese bioleaching, Chemosphere, 154, 628-639.

Gorbushina, A.A. (2007) Life on the rocks. Environmental Microbiology, 9, 1613-1631.

Graeser, S., Gabriel, W. (2013) Falottaite, IMA 2013-044. CNMNC Newsletter, No. 17, October 2013, page 3000. Mineralogical Magazine, 77, 2997-3005.

Graeser, G., Gabriel, W. (2016) Falottait (MnC2O4)·3H2O) - ein neues Oxalat-Mineral aus den Schweizer Alpen. Schweizer Strahler, 50, 20-27.

Huerta‐Rosas, B., Cano‐Rodriguez, I., Gamino‐Arroyo, Z., Gomez‐Castro, F.R., Carrillo‐Pedroza, F.R., Romo‐Rodriguez P., Gutierrez‐Corona J.F. (2020) Aerobic processes for bioleaching manganese and silver using microorganisms indigenous to mine tailings. World Journal of Microbiology and Biotechnology, 36, 124.

Huizing, A., Hal, H.A.M., Kwestroo, W., Langereis, C., Loosdregt, P.C. (1977) Hydrates of manganese (II) oxalate, MS. Res. Bull., 12, 505-511.

Izatulina, A.R., Gurzhiy, V.V., Frank-Kamenetskaya, O.V. (2014) Weddellite from renal stones: structure refinement and dependence of crystal chemical features on H_2O content. American Mineralogist, 99, 2–7.

Izatulina, A.R., Gurzhiy, V.V., Krzhizhanovskaya, M.G., Kuz'mina, M.A., Leoni, M., Frank-Kamenetskaya, O.V. (2018) Hydrated calcium oxalates: crystal structures, thermal stability and phase evolution. Crystal Growth & Design, 18, 5465−5478.

Johnson, J.E., Webb, S.M., Maa, C., Fischer, W.W. (2016) Manganese mineralogy and diagenesis in the sedimentary rock record. Geochimica et Cosmochimica Acta, 173, 210–231.

Kim, Y.-Y., Darkins, R., Broad, A., Kulak, A. N., Holden, M. A., Nahi, O., Armes, S. P., Tang, C. C., Thompson, R. F., Marin, F., Duffy, D. M., Meldrum, F. C. (2019) Hydroxyl-rich macromolecules enable the bioinspired synthesis of single crystal nanocomposites. Nature Communication, 10, 5682.

Kuz'mina, M.A., Rusakov, A.V., Frank-Kamenetskaya, O.V., Vlasov, D.Yu. (2019) The influence of inorganic and organic components of biofilm with microscopic fungi on the phase composition and morphology of crystallizing calcium oxalates. *Crystallography Reports*, 64, 161–167.

Madondo, J., Canet, C., González-Partida, E., Rodríguez-Díaz, A.A., Nú ñez-Useche, F., Alfonso, P., Rajabi, A., Pi, T., Blignaut, L., Vafeas, N. (2020) Geochemical constraints on the genesis of the 'Montaña de Manganeso'veintype Mn deposit, Mexican Plateau. Ore Geology Reviews.

Mehta, K.D., Chitrangada, D., Pandey, B.D. (2010) Leaching of copper, nickel and cobalt from Indian Ocean manganese nodules by *Aspergillus niger*. Hydrometallurgy, 105, 89–95.

Mills, S.J., Christy, A.G. (2016) The Great Barrier Reef expedition 1928–29: the crystal structure and occurrence of weddellite, ideally $CaC_2O_4 \cdot 2.5H_2O$, from the Low Isles, Queensland. Mineralogical Magazine, 80, 399-406.

Mulligan, C.N., Kamali, M., Gibbs, B.F. (2004) Bioleaching of heavy metals from a low-grade mining ore using Aspergillus niger. Journal of Hazardous Materials, 110, 77–84.

Milova-Ziakova, B., Uríka, M., Boriova, K., Bujdos, M., Kolencík, M., Mikusova, P., Takacova, A., Matús, P. (2016) Fungal solubilization of manganese oxide and its significance for antimony mobility fungal solubilization of manganese oxide and its significance for antimony mobility. International Biodeterioration and Biodegradation, 114, 157-163.

Mohanty, S., Ghosh, S., Nayak, S., Das, A.P. (2017) Bioleaching of manganese by *Aspergillus sp.* isolated from mining deposits. Chemosphere, 172, 302-309.

Morgan, J.J. (2005) Kinetics of reaction between O_2 and Mn(II) species in aqueous solutions. Geochimica et Cosmochimica Acta, 69, 35-48.

Mota, E. A., Felestrino, É. B., Leão, V. A., Guerra-Sá, R. (2020) Manganese (II) removal from aqueous solutions by *Cladosporium halotolerans* and *Hypocrea jecorina*. Biotechnology Reports, 25, 1-8.

Naganna, C. (1963) Thermal study of some manganese oxide and hydrous oxide minerals. Proceedings of the Indian academy of sciences - Section A, 58, 16–28.

Namgung, S., Chon, C.-M., Lee, G. (2018) Formation of diverse Mn oxides: a review of biogeochemical processes of Mn oxidation. Geosciences Journal, 22, 373- 381.

Pattnaik, S., Mukherjee, P., Barik, R., Mohapatra, M. (2019) Recovery of bi-metallic oxalates from low grade Mn ore for energy storage application. Hydrometallurgy, 189, 105-139.

Post. J. (1999) Manganese oxide minerals: Crystal structures and economic and environmental significance. Proc. Natl. Acad. Sci. USA, 96, 3447–3454.

Ren, W.-X., Li, P.-J., Geng, Y., Li, X.-J. (2009) Biological leaching of heavy metals from a contaminated soil by *Aspergillus niger*. Journal of Hazardous Materials, 167, 164–169.

Rusakov, A.V., Vlasov, A.D., Zelenskaya, M.S., Frank-Kamenetskaya, O.V., Vlasov, D.Yu. (2016) The crystallization of calcium oxalate hydrates formed by interaction between microorganisms and minerals. In O.V. Frank-Kamenetskaya, E.G. Panova, D.Yu. Vlasov, Eds., Biogenic—Abiogenic Interactions in Natural and Anthropogenic Systems, p.357-377. Springer International Publishing, Switzerland.

Rusakov, A.V., Kuzmina, M.A., Izatulina, A.R. and Frank-Kamenetskaya, O.V. (2019) Synthesis and Characterization of (Ca,Sr)[C2O4]_nH2O Solid Solutions: Variations of Phase Composition, Crystal Morphologies and in Ionic Substitutions. Crystals 9, 654.

Santelli, C.M., Webb, S.M., Dohnalkova, A.C., Hansel, C.M. (2011) Diversity of Mn oxides produced by Mn(II) oxidizing fungi. Geochimica et Cosmochimica Acta, 75, 2762‑2776.

Sayer, J.A., Kierans, M., Gadd, G.M. (1997) Solubilization of some naturally occurring metal-bearing minerals, limescale and lead phosphate by *Aspergillus niger*. FEMS Microbiology Letters, 154, 29-35.

Sazanova, K., Osmolovskaya, N., Schiparev, S., Yakkonen, K., Kuchaeva, L., Vlasov, D. (2014) Organic acids induce tolerance to zinc- and copper-exposed fungi under various growth conditions. Microbiology, 83, 1-9.

Seh-Bardan, B. J., Othman, R., Ab Wahid, S., Husin, A., Sadegh-Zadeh, F. (2012) Bioleaching of heavy metals from mine tailings by *Aspergillus fumigatus*. Bioremediation Journal, 16, 57–65.

Sheldrick, G.M. (2013) SADABS, University Gottingen, Germany.

Sheldrick, G.M. (2015a) SHELXT – Integrated space-group and crystal structure determination, Acta Crystallographica, 71, 3-8.

Sheldrick, G.M. (2015b) Crystal structure refinement with SHELXL. Acta Crystallographica, 71, 3-8.

Soleimannejad, J., Aghabozorg, H., Hooshmand, S., Ghadermazi, M., Gharamaleki, J.A. (2007) The monoclinic polymorph of catena-poly[[diaquamanganese(II)]-μ-oxalato-$\kappa^4O^1,O^2:O^{1'},O^{2'}$]. Acta Crystallographica Section Section E, 63, m2389-m2390.

Sterflinger, K. (2000) Fungi as Geological agents. Geomicrobiology Journal, 17, 97-124.

Sturm (nee Rosseeva), E.V., Frank-Kamenetskaya, O.V., Vlasov, D.Yu., Zelenskaya, M.S., Sazanova, K.V., Rusakov, A.V., Kniep, R. (2015) Crystallization of calcium oxalate hydrates by interaction of calcite marble with fungus *Aspergillus niger*. American Mineralogist,100, 2559-2565.

Tang, Y., Zeiner, C.A., Santelli, C.M., Hansel, C.M. (2013) Fungal oxidative dissolution of the Mn(II)-bearing mineral rhodochrosite and the role of metabolites in manganese oxide formation. Environmental Microbiology, 5, 1063–1077.

Tebo, B.M. (1991) Manganese(II) oxidation in the suboxic zone of the Black Sea. Deep Sea Research, Part A, 38, 883- 905.

Tebo, B.M., Johnson, H.A., McCarthy, J.K., Templeton, A.S. (2005) Geomicrobiology of manganese(II) oxidation. Trends in Microbiology, 13, 421–438.

Tsekova, K., Todorova, D., Ganeva, S. (2010) Removal of heavy metals from industrial wastewater by free and immobilized cells of *Aspergillus niger*. International Biodeterioration and Biodegradation, 64, 447-451.

Vlasov, D.Yu., Frank-Kamenetskaya, O.V., Zelenskaya, M.S., Sazanova, K.V., Rusakov, A.V., Izatulina, A R. (2020) The use of *Aspergillus niger* in modeling of modern mineral formation in lithobiotic systems. In: *Aspergillus niger*: Pathogenicity, Cultivation and Uses, Nova Science Publishers, New York, in press.

Warren, J. (1999) Conservation of Brick, 294 p. Butterworth Heinemann, Oxford

Wei, Z., Hillier, S., Gadd, G.M. (2012) Biotransformation of manganese oxides by fungi: solubilization and production of manganese oxalate biominerals. Environmental Microbiology, 14, 1744–1752.

Wilson, M.J., Jones, D. (1984) The occurrence and significance of manganese oxalate in *Pertusaria coralline* (Lichens). Pedobiologia (Jena), 26, 373-279.

Yao, S., Jin, B., Liu, Z., Shao, R., Zhao, C., Wang, X., Tang, R. (2017) Biomineralization: from material tactics to biological strategy. Advanced Materials, 29, 1605903.

Zak, L., Povondra, P. (1981) Kutnohorite from the Chvaletice Pyrite and Manganese Deposit, East Bohemia. TMPM Tschermaks Min. Petr. Mitt. 28, 55-63.

Zelenskaya, M.S., Rusakov, A.V., Frank-Kamenetskaya, O.V., Vlasov, D.Yu., Izatulina, A.R., Kuz'mina, M.A. (2020) Crystallization of calcium oxalate hydrates by interaction of apatites and fossilized tooth tissue with fungus *Aspergillus niger*. In O.V. Frank-Kamenetskaya, E.G. Panova, D.Yu. Vlasov, Lessovaia, S. Eds., Processes and phenomena on the boundary between biogenic and abiogenic nature, p. 581–603. Springer: Cham, Switzerland.

Fig.1. SEM images of the oxalate crystals formed on todorokite surface after 2 (a,b), 4(c,d), 6 (e,f), 8 (g,h), 14 (i,j) days of the experiment.

Fig.2. XRD patterns of oxalate crystals formed on todorokite surface after: a – 2, b – 6, c – 8, d – 14 days of the experiment. Wh – whewellite, Wd – weddellite, L – lindbergite, F – falottaite, T – todorokite.

Fig.3 SEM images of the oxalate crystals formed on kutnohorite surface after 2(a,b), 6(c,d), 8 (e), 14 (f) days of the experiment.

Fig.4. XRD patterns of oxalate crystals formed on kutnohorite surface after: a – 4, b – 6, c – 8, d - 14 days of the experiment. Wh – whewellite, Wd – weddellite, L – lindbergite, F – falottaite, T – biogenic Mn,Ca –oxide.

Fig.5. Powder XRD patterns of falottaite as a function of temperature (23 – 300 °C) on heating in air.

Fig. 6. Crystal structures of manganese oxalate hydrates: a – falottaite (sp. gr. *Pcca*), viewed along [010]; b – lindbergite (sp. gr. *C2/c*), viewed along [001]; c – falottaite, viewed along [100]; d – lindbergite, viewed along [010].

Fig.7. Phase assemblage of crystalline products of the reaction between Ca, Mn-minerals with *A. niger* versus pH of crystallization medium.

This is the peer-reviewed, final accepted version for American Mineralogist, published by the Mineralogical Society of America.
The published version is subject to change. Cite as Authors (Year) Title. American Mineralogist, in press.
DOI: https://doi.org/10.2138/am-2021-7651. http://www.minsocam.org/

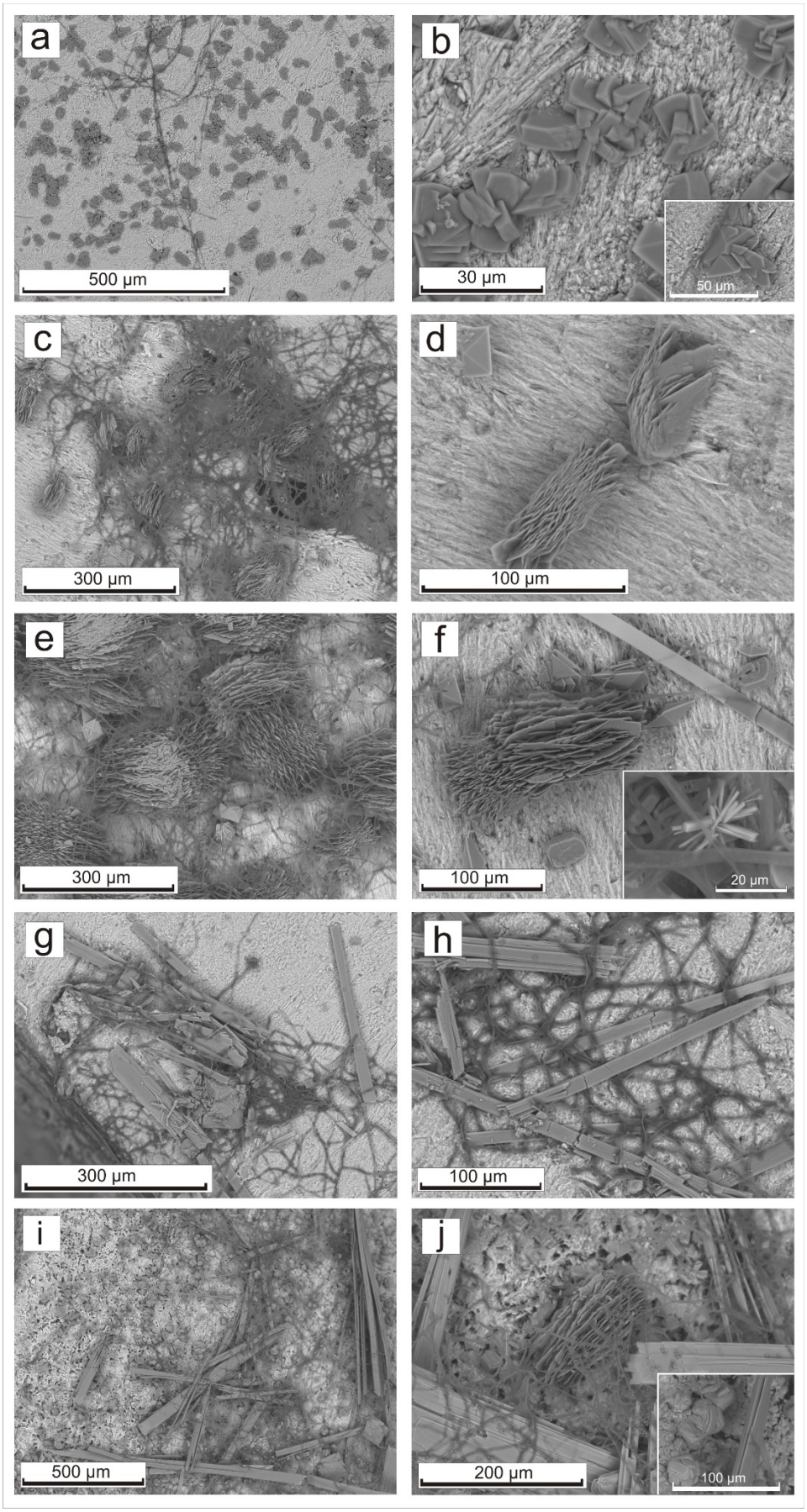

Fig.1. SEM images of the oxalate crystals formed on todorokite surface after 2 (a,b), 4(c,d), 6 (e,f), 8 (g,h), 14 (i,j) days of the experiment.

This is the peer-reviewed, final accepted version for American Mineralogist, published by the Mineralogical Society of America.
The published version is subject to change. Cite as Authors (Year) Title. American Mineralogist, in press.
DOI: https://doi.org/10.2138/am-2021-7651. http://www.minsocam.org/

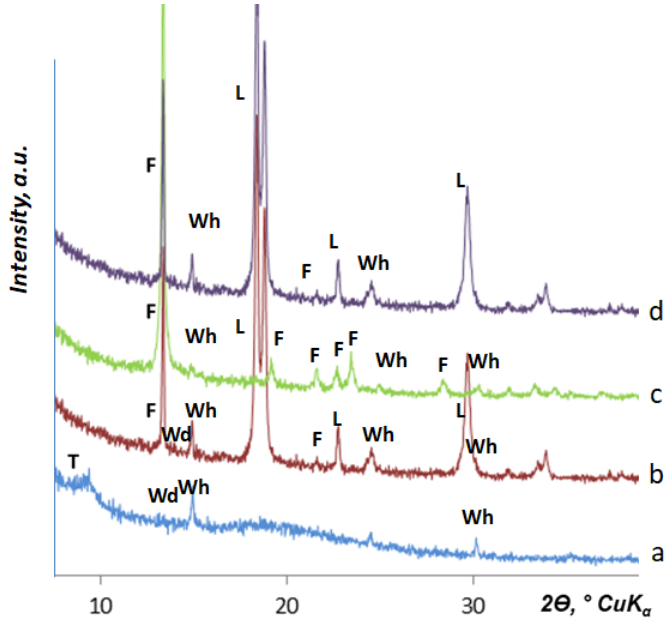

Fig.2. XRD patterns of oxalate crystals formed on todorokite surface after: a – 2, b – 6, c – 8, d – 14 days of the experiment. Wh – whewellite, Wd – weddellite, L – lindbergite, F – falottaite, T – todorokite.

This is the peer-reviewed, final accepted version for American Mineralogist, published by the Mineralogical Society of America.
The published version is subject to change. Cite as Authors (Year) Title. American Mineralogist, in press.
DOI: https://doi.org/10.2138/am-2021-7651. http://www.minsocam.org/

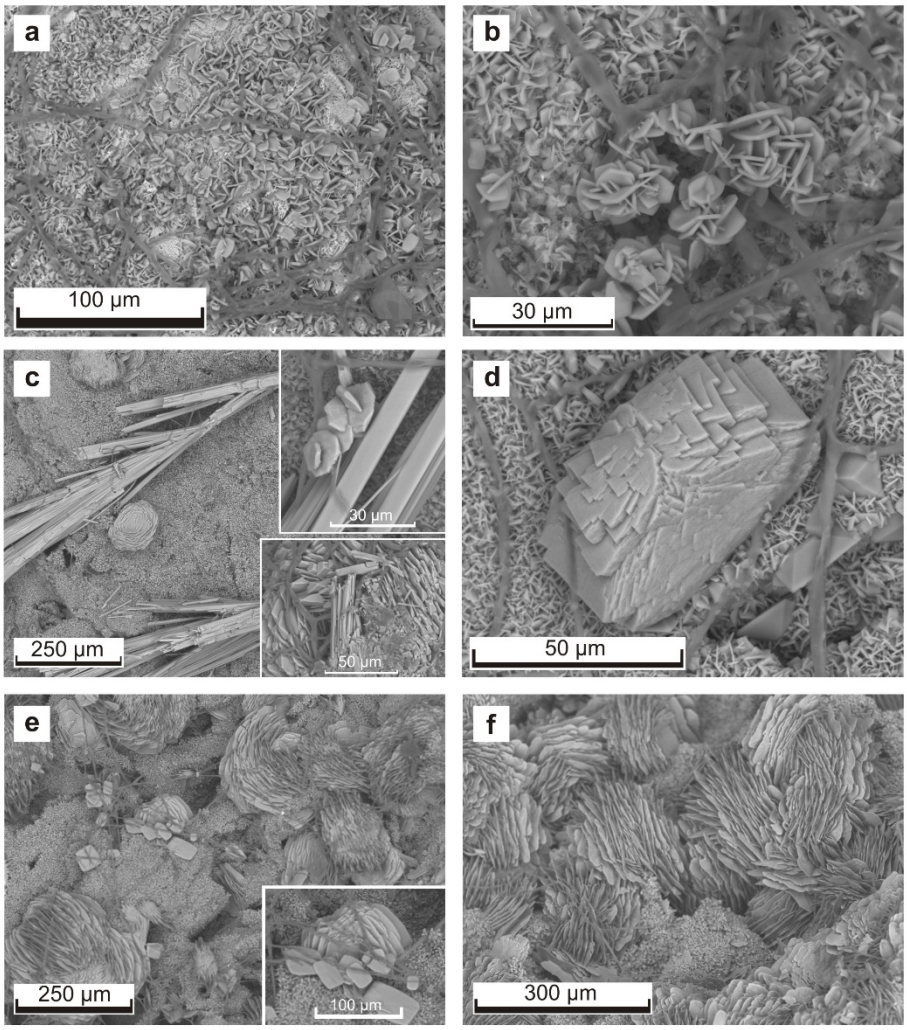

Fig.3 SEM images of the oxalate crystals formed on kutnohorite surface after 2 (a,b), 6 (c,d), 8 (e), 14 (f) days of the experiment.

This is the peer-reviewed, final accepted version for American Mineralogist, published by the Mineralogical Society of America.
The published version is subject to change. Cite as Authors (Year) Title. American Mineralogist, in press.
DOI: https://doi.org/10.2138/am-2021-7651. http://www.minsocam.org/

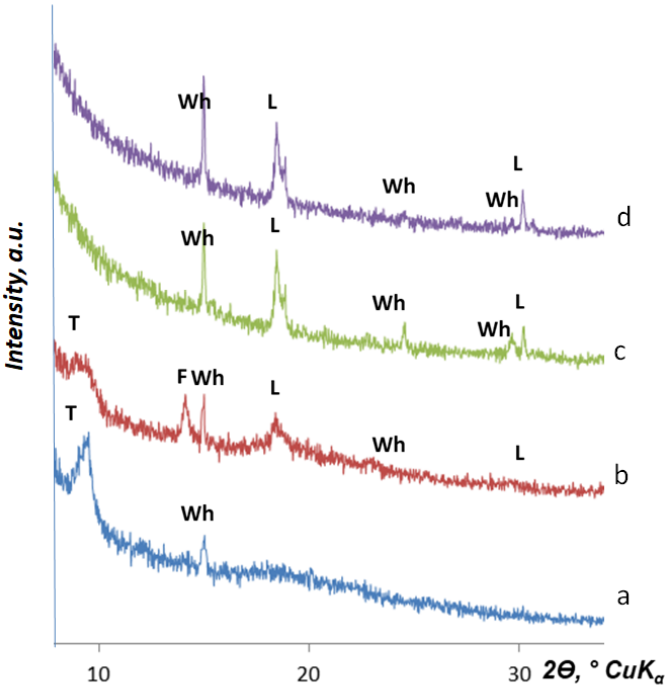

Fig.4. XRD patterns of oxalate crystals formed on kutnohorite surface after: a – 4, b – 6, c – 8, d - 14 days of the experiment. Wh – whewellite, Wd – weddellite, L – lindbergite, F – falottaite, T – biogenic Mn,Ca –oxide.

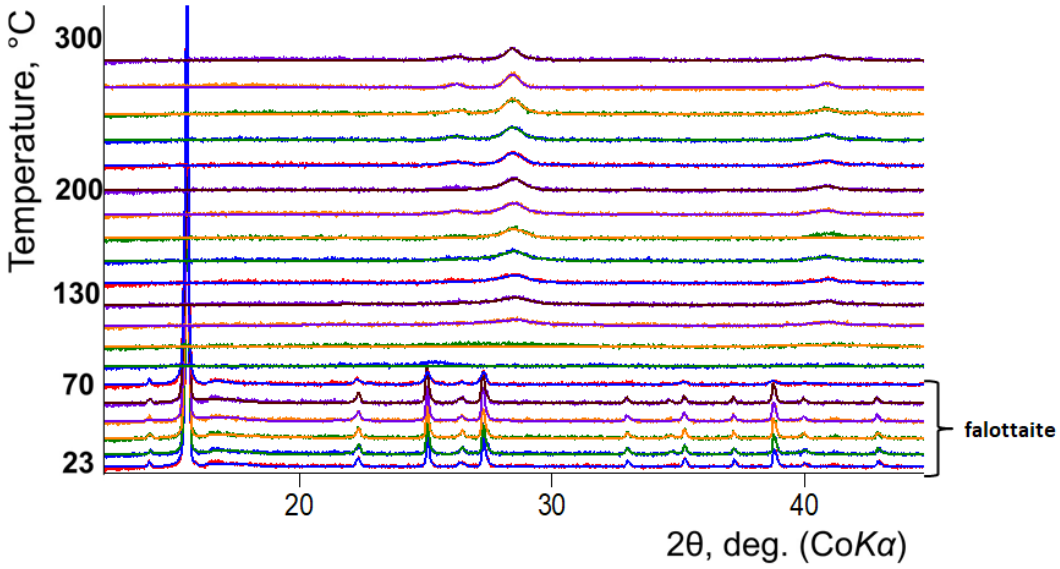

Fig.5. Powder XRD patterns of falottaite as a function of temperature (23 – 300 °C) on heating in air.

This is the peer-reviewed, final accepted version for American Mineralogist, published by the Mineralogical Society of America.
The published version is subject to change. Cite as Authors (Year) Title. American Mineralogist, in press.
DOI: https://doi.org/10.2138/am-2021-7651. http://www.minsocam.org/

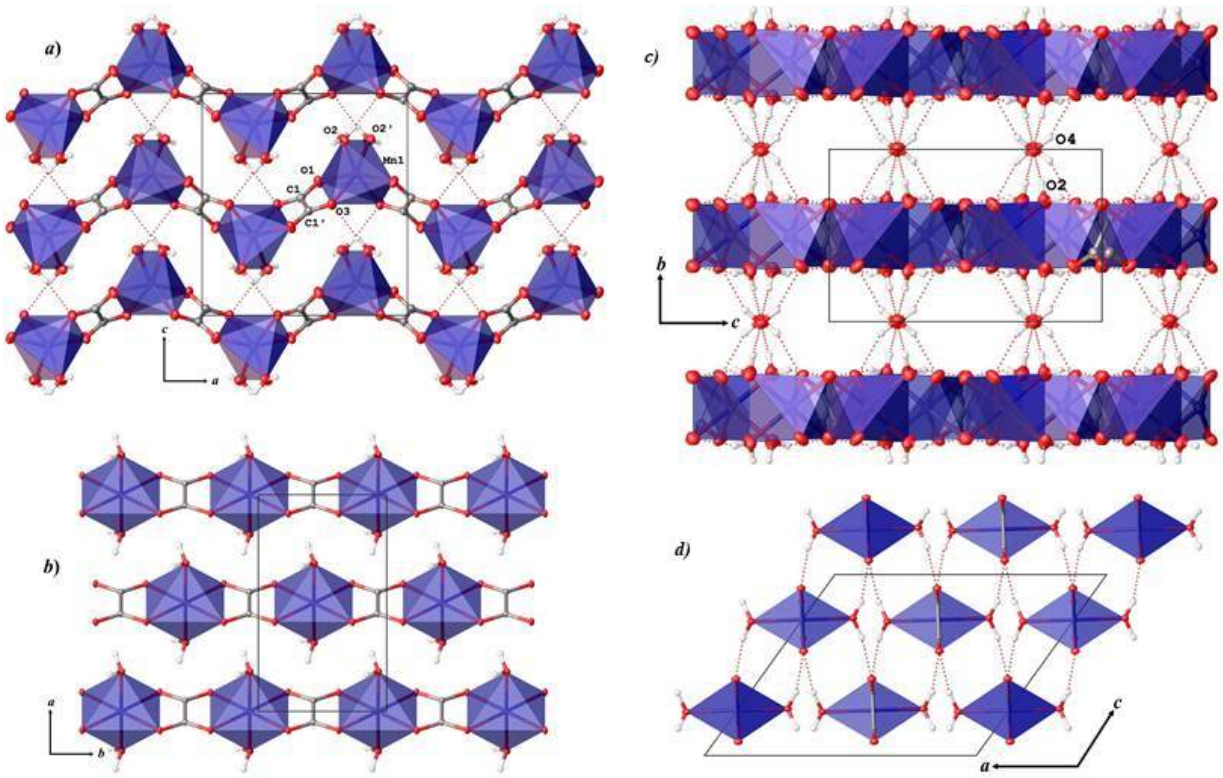

Fig. 6. Crystal structures of manganese oxalate hydrates: a – falottaite (sp. gr. *Pcca*), viewed along [010]; b – lindbergite (sp. gr. *C2/c*), viewed along [001]; c – falottaite, viewed along [100]; d – lindbergite, viewed along [010].

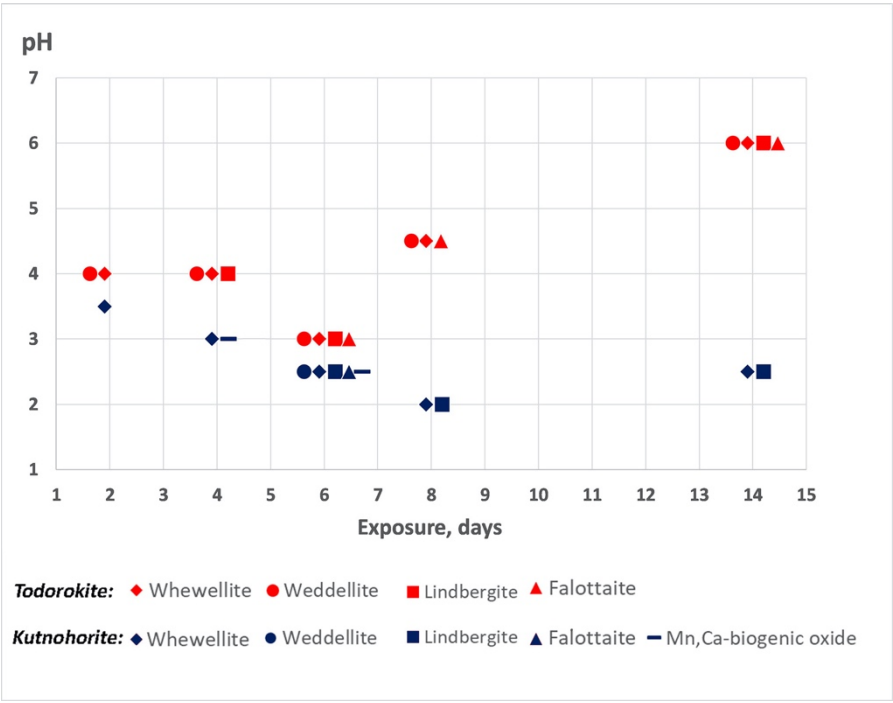

Fig.7. Phase assemblage of crystalline products of the reaction between Ca, Mn-minerals with *A. niger* versus pH of crystallization medium.

This is the peer-reviewed, final accepted version for American Mineralogist, published by the Mineralogical Society of America.
The published version is subject to change. Cite as Authors (Year) Title. American Mineralogist, in press.
DOI: https://doi.org/10.2138/am-2021-7651. http://www.minsocam.org/

Table1. Crystallographic data and selected refinement parameters for the studied biogenic falottaite (manganese oxalate trihydrate).

Formula	$[Mg_{0.15}Mn_{0.85}(C_2O_4)(H_2O)_2]\cdot(H_2O)$
a (Å)	9.7559(10)
b (Å)	6.6259(7)
c (Å)	10.5198(11)
α(°)	90
β (°)	90
γ(°)	90
V (Å^3)	680.02(12)
Formula mass	192.49
Space group	*Pcca*
μ (mm^{-1})	1.926
Temperature (°C)	293(2)
Z	4
D_{calc} (g/cm^3)	1.678
Size (mm^3)	0.16×0.06×0.02
Radiation	Mo$K\alpha$
Total ref.	6817
Unique ref.	786
2θ range, °	6.15–55.00
Unique $\|F_o\| \geq 4\sigma_F$	585
R_{int}	0.0466
R_σ	0.0304
R_1 ($\|F_o\| \geq 4\sigma_F$)	0.0190
wR_2 ($\|F_o\| \geq 4\sigma_F$)	0.0320
R_1 (all)	0.0337
wR_2 (all)	0.0339
GOF	0.848
ρ_{min}, ρ_{min}, e/Å^3	–0.179, 0.262
Note: $R_1 = \sum\|\|F_o\| - \|F_c\|\|/\sum\|F_o\|$; $wR_2 = \{\sum[w(F_o^2 - F_c^2)^2]/\sum[w(F_o^2)^2]\}^{1/2}$; $w = 1/[\sigma^2(F_o^2) + (aP)^2 + bP]$, where $P = (F_o^2 + 2F_c^2)/3$; GOF = $\{\sum[w(F_o^2 - F_c^2)]/(n-p)\}^{1/2}$ where	

n is the number of reflections and *p* is the number of refined parameters.

Table 2. Cation composition of todorokite and kutnohorite

	Todorokite	Kutnohorite	Todorokite	Kutnohorite
Cation content, wt. %			Cation content in formula, apfu	
Mn	59,41	28,22	5.53	0.97
Na	1,62	0	0.36	0
Ca	0,69	16,37	0.09	0.77
Fe	0	4,18	0	0.14
Mg	2,23	1,40	0.47	0.11
Sr	0,59	0	0.03	0
Ba	0,43	0	0.02	0
K	0,42	0	0.06	0

Table 3. Relative abundance of the crystalline products of the reaction between Ca, Mn-minerals with *A. niger* versus pH of crystallization medium

Days	Todorokite		Kutnohorite	
	Phase composition	pH	Phase composition	pH
2	Wh*>>Wd*	4	Wh	3,5
4	Wh>>Wd, L*	4	Wh, Mn,Ca biogenic oxide	3
6	Wh>>Wd, L>F*	3	Wh>>Wd, L=F, Mn,Ca biogenic oxide	2,5
8	Wh>>Wd, F	4,5	Wh, L	2
14	Wh>>Wd, F=L	6	Wh, L	2,5

*Wh – whewellite, Wd – weddellite, L – lindbergite, F – falottaite